High Dynamic Range Image Watermarking Based on Tucker Decomposition

MEI YU, YANG WANG, GANGYI JIANG⬡, (Senior Member, IEEE), **YONGQIANG BAI, AND TING LUO**⬡
Faculty of Information Science and Engineering, Ningbo University, Ningbo 315211, China
Corresponding author: Gangyi Jiang (gyjiang@nbu.edu.cn)

ABSTRACT High dynamic range (HDR) imaging technique has received much attentions in the recent years for its abundant details and wide dynamic range of luminance. In order to display HDR images on low dynamic range display devices, tone mapping (TM) process is required. However, the TM can be deemed as an inevitable attack in the field of HDR image copyright protection. In this paper, a highly robust HDR image watermarking algorithm based on Tucker decomposition is proposed. Firstly, Tucker decomposition is carried out on HDR color image to obtain the first feature map of the core tensor, which contains most of the energies in the HDR host image. Then, a Auto-Regressive prediction method is used to establish a local correlation model of the first feature map, so that watermark can be embedded in the first feature map according to the prediction result and its true value. Furthermore, a low-complexity luminance masking approach is designed based on modified specular free map to exclude the areas not suitable for watermark embedding, and an embedding intensity selection strategy is used to balance the imperceptibility and robustness of the watermark. The experimental results show that the proposed algorithm is robust against existing TM attacks while keeping better image imperceptibility and embedding capacity.

INDEX TERMS High dynamic range image, digital watermarking, tone mapping, tucker decomposition, luminance mask.

I. INTRODUCTION

With the wide applications of high dynamic range (HDR) imaging technology [1]–[3] in the field of consumer electronics, video production, virtual reality, remote sensing, medical detection, HDR image copyright protection has also received increasing attentions. In contrast to the traditional low dynamic range (LDR) images, the dynamic range of HDR images can generally reach or exceed 9 orders of magnitude [4], which can not only improve the accuracy of scene brightness information to a certain extent, but also bring abundant color details and renditions of shading gradations. HDR imaging technology commonly employs floating-point type numbers to represent and store HDR images [5]. Since the existing LDR display devices have a much more limited dynamic range, tone mapping (TM) [6] process is required if HDR images with rich details are to be displayed on an LDR display device. However, for copyright protection

of HDR images, the TM process is undoubtedly a unique and inevitable form of attack. Additionally, TM is a nonlinear mapping process, HDR images with watermark exhibit different robustness in different luminance areas after TM processing. Although traditional LDR image watermarking technology is maturing [7], considering the characteristics of HDR images and the nonlinear characteristics of TM attacks, the traditional watermarking methods are difficult to achieve better performance if simply transplanted to HDR images. Therefore, it is important to design robust HDR image watermarking algorithm against TM attacks.

Currently, there are two main categories of HDR image watermarking technology depending on their different purposes: The first is fragile watermarking, which pays more attention to invisibility and embedding capacity, and often embeds watermark in spatial domain of the images. Yu *et al.* [8], Wang *et al.* [9] and Chang *et al.* [10], [11] employed the exponential channel of HDR image with RGBE storage format to realize the lossless watermark embedding. Cheng *et al.* [12] and Li *et al.* [13] combined the least

---

The associate editor coordinating the review of this article and approving it for publication was Md. Asikuzzaman.

significant bit (LSB) approach to embed the watermark in HDR image with RGBE format or LogLuv (TIFF) format, respectively. Lin *et al.* [14] used the 10-digit mantissa in OpenEXR format to convey secret information. The other is robust watermarking, which considers the content characteristics of HDR images itself, and usually embeds the watermark in transform domain of the image. Guerrini *et al.* [15] designed a visual perceptual mask based on luminance, texture and edge information to enhance the imperceptibility, and employed the quantization index modulation (QIM) technique to embed the watermark in the low-frequency-band of the discrete wavelet transformation (DWT) domain with the kurtosis as features. Furthermore, the algorithm was tested on 15 HDR images with 7 TM attacks, and achieved better imperceptibility, but the average bit error rate (BER) reached 29%. Xue *et al.* [16] proposed two different schemes, one in which employed the μ-law to characterize a general TM, and applied it to HDR image to derive an LDR representation where the watermark can be embedded, the other in which applied bilateral filtering to HDR images to obtain the detail part where watermark can be embedded. Both of the schemes employed spread-spectrum approach to insert the watermark into DWT domain, and achieved better performance in imperceptibility according to a limited set of test images, but the robustness was still poor. Wu *et al.* [17] embedded watermark into discrete cosine transform (DCT) domain of LDR images processed by a special TM for HDR images, thus the algorithm was only robust for the pre-determined TM attack. Solachidis *et al.* [18] proposed that the original HDR image was decomposed into a set of LDR images with different exposure by means of a bracketing process, and the watermark was embedded into DWT domain of the image sequence. However, even though the idea of several times embedding resulted in a better robustness, it also brought a poor imperceptibility at the same time. Then at the same year, Solachidis *et al.* [19] employed wavelet transform in Just Noticeable Difference (JND)-scaled space of the original HDR image as the embedding domain, and employed the contrast sensitivity function (CSF) to modulate the embedding intensity. This algorithm exhibited a better robustness against 7 TM attacks, but the embedding capacity was only 128 bit. Maiorana *et al.* [20] performed the logarithm, DWT, block and Radon DCT (RDCT) processing on luminance component of HDR images in turn, and then a QIM watermarking process was applied. The algorithm tested 15 HDR images under 6 TM attacks, which showed a better imperceptibility, but the average BER was about 20%. Anbarjafari *et al.* [21] combined the characteristics of DWT, chirp z-transform (CZT), QR-decomposition and singular value decomposition (SVD) to embed watermark, which exhibited a better robustness against 14 TM attacks, however, the watermark extraction was non-blind. Bai *et al.* [22] proposed a robust HDR image watermarking algorithm based on spatial activity, employed the non-subsampled contourlet transform (NSCT) and SVD to extract structural information of HDR images where the watermark can be embedded.

Furthermore, the hierarchical embedding intensity and hybrid perceptual mask was designed to optimize the robustness and imperceptibility. The algorithm performed a better robustness against 27 TM attacks.

In summary, the existing robust HDR image watermarking algorithms have achieved some successes against a few TM attacks. But it still has the following inadequacies. One is that the traditional image processing method usually converts the high-dimension image data into vectors or matrices form by using DCT, DWT, RDWT, NSCT, SVD, etc., which not only causes too high dimension of data sample, but also destroys the internal structure of the data itself. The other is that the TM is a nonlinear mapping process, i.e. the image exhibits different robustness in different luminance areas after TM attack.

Considering that tensor not only can naturally represent high-dimension data, but also can effectively solve the problem of internal structure destructed in the traditional image processing method, a highly robust HDR image blind watermarking algorithm based on tensor decomposition [23] against TM attacks is proposed in this paper. Two major contributions of the paper are summarized as follows. (1) In order to avoid the quality degradation of watermarked image resulted from single channel embedding and inaccurate prediction, the HDR color image is first regarded as a third-order tensor, and Tucker decomposition is employed to obtain the first feature map of the core tensor, which has high stability and contains most of the energies in the HDR host image, and thus is selected as the carrier of watermark. Additionally, an Auto-Regressive (AR) [24] prediction method is used to establish a local correlation model of the first feature map to improve the prediction accuracy, so that watermark can be embedded in the first feature map according to the prediction result and its true value. (2) Considering the nonlinear characteristics of TM attacks, we refer the specularity removal technique in LDR image and design a low-complexity luminance masking approach based on the modified specular free (MSF) [25] to optimize the robustness of watermarking. Furthermore, in order to make the compromise between the imperceptibility and robustness, and to adaptively select embedding intensity for different HDR host images, an embedding intensity selection strategy is proposed.

The rest of the paper is organized as follows: in section 2, prior knowledge of the proposed algorithm in the implementation process are first introduced, and then the proposed HDR image watermarking algorithm based on Tucker decomposition is described in detail. The experimental results are illustrated in section 3 and finally, the conclusion of the paper is brought in section 4.

II. PROPOSED HDR IMAGE WATERMARKING ALGORITHM

In this paper, a highly robust HDR image watermarking algorithm is proposed, which takes advantage of the facts that tensor decomposition does not destroy the internal structure

of data, and can effectively diffuse the embedded watermark into three channels of the HDR host images through its inverse operation, so that the robustness and imperceptibility of the watermark can be improved. Firstly, HDR color image is regarded as a third-order tensor, on which Tucker decomposition is carried out to obtain the first feature map of the core tensor that contains most energies of the host image. Then, a luminance mask is obtained with MSF map to determine the regions suitable for embedding watermark. Finally, a local correlation model is used to predicate the value of center pixel of each block of the first feature map, and the watermark is embedded in each block according to the real value of the center pixel and its predicted result, during which an embedding intensity selection strategy is adopted to balance the imperceptibility and robustness.

A. TUCKER DECOMPOSITION FOR HDR IMAGE

For high-dimensional data, the classical data processing method is to convert it into vectors or matrices, which will lead to high dimension of data samples and destroy the structure of data. However, tensor decomposition can effectively overcome these problems. Currently, there are two commonly used factored forms of tensor decomposition. The first is the canonical polyadic (CP) decomposition which represents a tensor as the weighted sum of finite rank-one tensors. The second is Tucker decomposition which is a high-order principal component analysis method and can decompose the original tensor into a product of the core tensor and a series of orthogonal matrices. Furthermore, the core tensor has a high stability and retains the mainly information in the original tensor.

In tensor algebra, for any tensor $\mathcal{A} \in R^{I_1 \times I_2 \times \cdots \times I_n}$, it can be decomposed into n-mode product by Tucker decomposition. The original tensor $\mathcal{A}$ and the core tensor $\mathcal{B}$ satisfy the following relationships:

$$\mathcal{A} = \mathcal{B} \times_1 U^{(1)} \times_2 U^{(2)} \times_3 U^{(3)} \times \cdots \times_n U^{(n)}$$
$$\Updownarrow$$
$$\mathcal{B} = \mathcal{A} \times_1 (U^{(1)})^T \times_2 (U^{(2)})^T \times_3 (U^{(3)})^T \times \cdots \times_n (U^{(n)})^T \tag{1}$$

where $I_1, \ldots,$ and I_n represent the number of elements in each dimension, $U^{(i)}$ is the orthogonal matrix, the superscript T represents matrix transposition.

In this paper, the HDR color image with three dimensional data is transformed by using Tucker decomposition along the RGB channels. The first feature map is selected as the watermark embedding carrier, because it covers the major energies of the HDR host image, and it is easy to diffuse the embedded watermark into three RGB channels of the watermarked image with inverse Tucker decomposition. Thus, the robustness of watermark is improved and the correlation of the multidimensional data is preserved. The steps of obtaining the first feature map of core tensor are described as follows:

Step1: Regard an HDR color image with RGB channels as a third-order tensor, i.e. $\mathcal{A} \in R^{I_1 \times I_2 \times I_3}$, where the I_1, I_2

and I_3 represent the height, width and color information of the image, respectively, then expand it along the ith dimension to obtain the expansion matrix $A_{(i)}(i = 1, 2, 3)$.

Step2: Perform SVD on the expansion matrix $A_{(i)}$ to obtain the orthogonal matrix $U^{(i)}$.

Step3: Construct the core tensor $\mathcal{B}$ with the orthogonal matrix of mode-3 $U^{(3)}$ and the original tensor $\mathcal{A}$ according to Eq.(1). Thus the first feature map Q_1 of core tensor is obtained, where Q_1, Q_2 and Q_3 denote the first, second and third feature maps, respectively. $\|\mathcal{A}\| = \|\mathcal{B}\| = \sum_{i=1}^{3} \|Q_i\|^2$ and $\|Q_1\| \geq \|Q_2\| \geq \|Q_3\|$, and symbol $\| \cdot \|$ is the F-norm.

B. LOCAL CORRELATION MODEL BASED ON AR PREDICTION METHOD

AR prediction is an effective statistical method for time-series and is widely applied to various areas of forecasting such as signal processing, state estimation, pattern recognition, etc. It achieves the goal of error ε minimization by maximizing Bayesian conditional probability between input point and its adjacent points. Furthermore, it shows higher accuracy compared with conventional 4 or 8 neighborhood prediction methods. In this paper, to solve the problem of imperceptibility reduction caused by inaccurate prediction in subsequent watermark embedding process to some extent, AR prediction is used to establish the local correlation between the center pixel $A_{i,j}$ of a block and its adjacent pixels $A_{i+m,j+n}$ of the first feature map of the core tensor, and the AR coefficients are denoted as the local correlation model of the image. Before watermark embedding of an HDR image, the AR model of the host image needs to be trained with the image's coefficients of the first feature map Q_1. Meanwhile, the model is delivered as the secret Key2 to improve the accuracy and security of watermark extraction. The AR model is denoted by

$$A_{i,j} = \sum_{m=-k}^{k} \sum_{n=-k}^{k} A_{i+m,j+n} \times \alpha_{m,n} + \varepsilon \tag{2}$$

where m and n are not simultaneously 0, $A_{i,j}$ denotes the pixel value of the location (i, j) in the first feature map, k denotes the extent of the neighborhood used for predicting $A_{i,j}$ and it is set to 2 in this paper, therefore, there are total 24 AR coefficients used as the secret Key2. ε is the error term, $\alpha_{m,n}$ denotes the AR coefficient of corresponding location and reflects the correlation between $A_{i,j}$ and its adjacent pixels $A_{i+m,j+n}$.

C. LUMINANCE MASK

Through analyzing global TM operators, the mapping function can be approximately represented as shown in Figure 1, where the horizontal axis represents the dynamic range of HDR image, i.e. $d \in [0, 9]$, and the vertical axis represents the normalized pixel value of tone-mapped image, i.e. $P \in [0, 1]$. Obviously, this is a nonlinear mapping process, with the increase of dynamic range, the slope decreases obviously. Although the existing TMs also include local TM operator
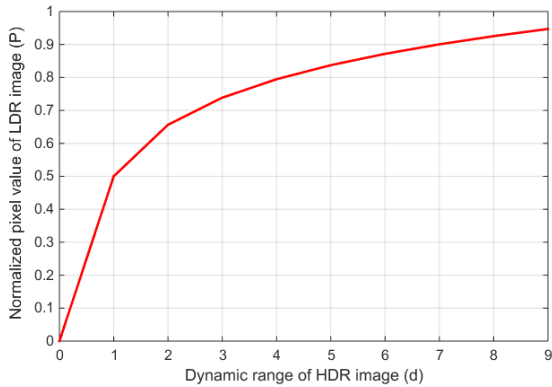
FIGURE 1. Schematic illustration of TM curve.

that adjusts mapping parameters according to local information of HDR image, considering that the goal of all TMs is to compress the dynamic range of HDR images, it is a reasonable hypothesis that pixel values in different luminance areas of an HDR image have different compression ratios for both global and local TM operators. From the curve such as shown in Figure 1, the nonlinear characteristics of TMs will cause the orders of magnitude fluctuating for values of different luminance areas. This will lead to different robustness in different luminance areas for watermarked HDR images, i.e. the watermark in low-luminance areas increases with enlarging pixel values of images, while the watermark in high-luminance areas decreases or even loses with compressing pixel values of images. Therefore, to solve the problem of poor robustness in high-luminance areas, a MSF based low-complexity luminance masking approach is designed to exclude the areas not suitable for embedding watermark. The mask extraction is as follows:

Step1: Calculate the specular-free (SF) image for the HDR image.

$$SF_c(x, y) = I_c(x, y) - \min\left(I_r(x, y), I_g(x, y), I_b(x, y)\right) \quad (3)$$

Step2: Obtain the MSF image by adding the mean of the minimum value of the three RGB channels of the host image to the SF image.

$$MSF_c(x, y) = SF_c(x, y) + \bar{I}_{\min} \quad (4)$$

Step3: Calculate the difference image between the host image and MSF image by using Eq. (5). Then binarization is performed by using Eq. (6).

$$d(x, y) = \frac{1}{3} \times \left(\sum_c (I_c(x, y) - MSF_c(x, y))\right) \quad (5)$$

$$Mask(x, y) = \begin{cases} 0, & if \ d(x, y) > th \\ 1, & otherwise \end{cases} \quad (6)$$

Step4: Finally, down-sampling and morphological processing are performed in accordance with the size of block to obtain the luminance mask.

In the above formulas, $c \in \{r, g, b\}$, $I_c(x, y)$ is the value of the c color channel at location (x, y) of the host image, $I_{\min}(x, y) = \min\left(I_r(x, y), I_g(x, y), I_b(x, y)\right)$. $\bar{I}_{\min}$ is the mean of the minimum value $I_{\min}(x, y)$. th is a threshold that is found for each image by Nobuyuki Otsu (OTSU) method. *Mask* represents the luminance mask for high-luminance areas.

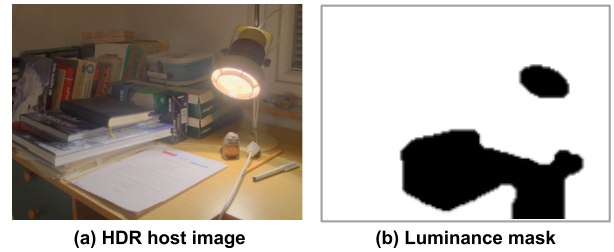(a) HDR host image   (b) Luminance mask

FIGURE 2. HDR host image and its luminance mask.

For ease of observation, Figure 2 shows an HDR host image and its luminance mask obtained by the proposed luminance masking approach, wherein the black areas represent the high-luminance areas which are not suitable for watermark embedding, and only the white areas are selected as the carrier in this paper.

D. EMBEDDING INTENSITY SELECTION STRATEGY

Under the premise of a certain embedding capacity, in order to adaptively select the optimal embedding intensity for different HDR host images so as to make balance between robustness and imperceptibility of watermark, an embedding intensity selection strategy is proposed as shown in Figure 3. Firstly, the watermarked HDR images with respect to different embedding intensities are obtained by using the proposed watermarking algorithm. Then, the imperceptibility index (i.e. visible difference predictor (VDP)) and the robustness against several typical TM attacks (i.e. BER) under each
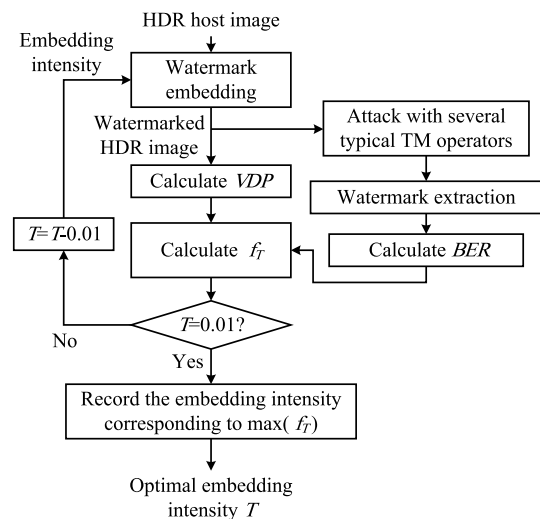

FIGURE 3. Flowchart of embedding intensity selection.

embedding intensity are calculated. Finally, the function f_T is calculated according to Eq. (7), and the intensity T corresponding to max(f_T) is taken as the optimal embedding intensity for the host image.

$$f_T = VDP_T + \frac{1}{5} \times \sum_{i=1}^{5} BCR_{T,i} \qquad (7)$$

where $BCR_{T,i} = 100\text{-}BER_{T,i}$, VDP_T denotes the objective quality evaluation index under embedding intensity T, $BER_{T,i}$ represents the bit error rate (%) of extraction under the ith attack type when the embedding intensity is T. The range of VDP and BCR (%) are from 0 to 100. The initial value of the intensity T is 0.5, the decrementing step is 0.01, and the attack types chosen for the selection strategy include five commonly used TMs, that is, Drago, Durand, Fattal, PattanaikVisual and ReinhardDevlin TM operators which come from the HDR Toolbox for Matlab [26].

Taking the HDR host image in Figure 2(a) as an example, Figure 4 shows the variation curves of VDP, average BCR (processed by the 5 TM attacks) and the function f_T under different embedding intensity for this image. It can be found from Figure 4 that f_T takes the maximum value when T is equal to 0.05. Thus, 0.05 is taken as the optimal embedding intensity for this host image.
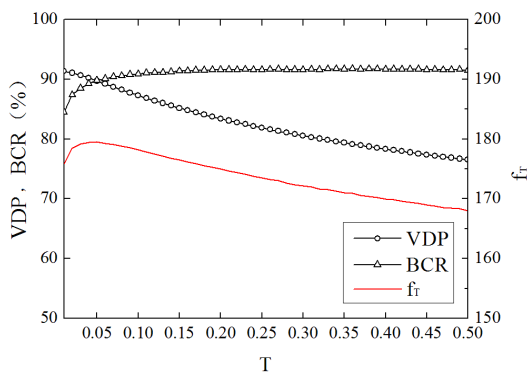

FIGURE 4. f_T curve of HDR host image.

E. PROPOSED HDR IMAGE WATERMARKING ALGORITHM

Based on Tucker decomposition, local correlation model, luminance mask and embedding intensity selection strategy discussed above, we proposed a new watermarking algorithm for HDR color images against TM attacks. Firstly, HDR host image is processed with Tucker decomposition, and the first feature map Q_1 is obtained. Then, the local correlation model based on the auto-regressive prediction method is constructed for the first feature map. Finally, watermark is adaptively embedded by using the luminance mask and the optimal embedding intensity according to the real and predicated values of center pixel of blocks of the first feature map. The watermark extraction is the reverse of the watermark embedding.
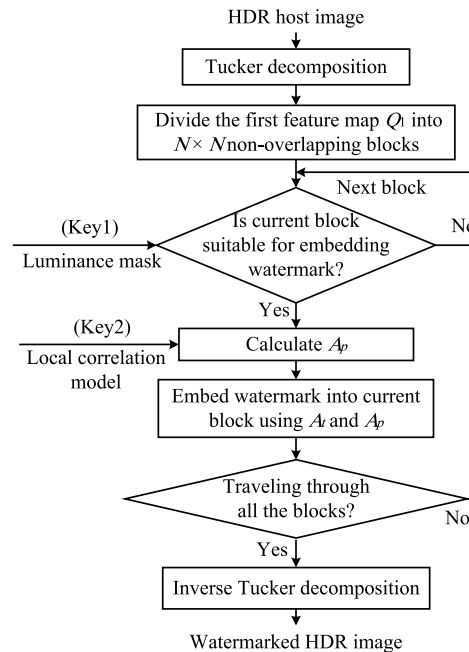

FIGURE 5. Flowchart of watermark embedding process.

The flowchart of the embedding process is illustrated in Figure 5, and the steps with more details are as follows:

Step1: The HDR host image is processed with Tucker decomposition so that the first feature map Q_1 is obtained, which will then be divided into a number of $N \times N$ non-overlapping blocks.

Step2: For each $N \times N$ block, determine whether it is suitable for watermark embedding by using the luminance mask which is used as Key1. If it is, Step3 is performed, otherwise, judge the next block until all blocks have been processed and then go to Step4.

Step3: Use Eq. (8) to embed the watermark, where A_t represents the real value of the center pixel of the block, while A_p is the value of the center pixel predicted with the local correlation model (Key2) using its adjacent pixels, T is the optimal embedding intensity obtained with the embedding intensity selection strategy, w represents one bit watermark to be embedded, $|\cdot|$, max($\cdot$) and sign($\cdot$) represent the absolute value, maximum value and sign value, respectively. After the watermark w is embedded, turn to Step2 to process the next block.

$$A_t^w = \begin{cases} \text{sign}(A_t) \times \max\left(|A_t|, |A_p| \times (1+T)\right), & \text{if } w = 1 \\ \text{sign}(A_t) \times \min\left(|A_t|, |A_p| \times (1-T)\right), & \text{otherwise} \end{cases}$$
$$(8)$$

Step4: Perform the inverse Tucker decomposition to obtain the watermarked HDR image.

Figure 6 gives flowchart of watermark extraction of the proposed algorithm, which consists of the following steps:

Step1: The watermarked image is processed with Tucker decomposition to obtain its first feature map Q_1, which will be divided into a number of $N \times N$ non-overlapping blocks.

TABLE 1. The 30 test HDR host images [27]–[29].

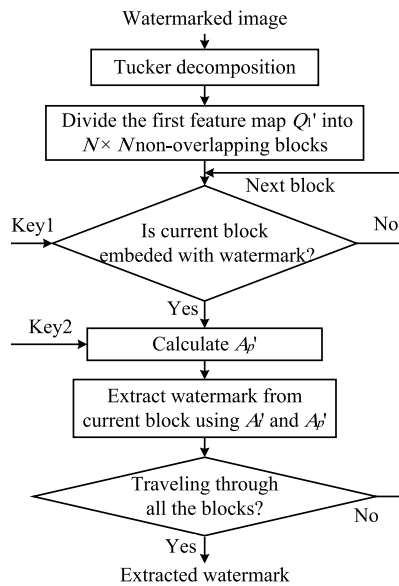| Image ID	Image Name	Size	Reference	Notes	Image ID	Image Name	Size	Reference	Notes
1	Apartment	2048×1536	[27]	Nature, indoor	16	SpheronNapaValley	3025×2129	[27]	Nature, outdoor
2	AtriumNight	760×1016	[27,28]	Nature, indoor	17	SpheronNice	2981×1165	[27]	Nature, outdoor
3	bigFogMap	751×1130	[27]	Nature, outdoor	18	SpheronPriceWestern	3272×1280	[27]	Nature, outdoor
4	dani_belgium	1025×768	[27]	Nature, indoor	19	Tree	928×906	[27]	Nature, outdoor
5	Desk	644×874	[27]	Nature, indoor	20	AtriumMorning	760×1016	[28]	Nature, indoor
6	Display1000	2048×1536	[27]	Nature, outdoor	21	Iwate	3720×1396	[28]	Nature, outdoor
7	memorial	512×768	[27]	Nature, indoor	22	mpi_atrium_1	1024×676	[28]	Nature, indoor
8	Montreal	2048×1536	[27]	Nature, outdoor	23	nancy_cathedral_1	1536×2048	[28]	Nature, indoor
9	nave	720×480	[27]	Nature, indoor	24	nancy_cathedral_2	1536×2048	[28]	Nature, indoor
10	rend01	1024×1024	[27]	Artificial	25	snow	2048×1536	[28]	Nature, outdoor
11	rend07	575×575	[27]	Artificial	26	2	713×535	[29]	Nature, outdoor
12	rend09	1024×1024	[27]	Artificial	27	3	357×535	[29]	Nature, indoor
13	rend10	1024×1024	[27]	Artificial	28	9	713×535	[29]	Nature, outdoor
14	rend13	1024×1024	[27]	Artificial	29	14	713×535	[29]	Nature, indoor
15	rosette	720×480	[27]	Nature, indoor	30	15	401×535	[29]	Nature, outdoor

FIGURE 6. Flowchart of watermark extraction process.

Step2: For each $N \times N$ block, determine whether it is embedded with watermark according to Key1. If it is, then turn to Step3 to extract the embedded watermark; otherwise, judge the next block until all blocks have been processed and then turn to Step4.

Step3: Let A'_t and A'_p be the real value and predicted value of the center pixel of the block calculated using Key2, the watermark embedded in the block can be extracted by using Eq. (9). Turn to Step2 to process the next block.

$$w' = \begin{cases} 1, & if \ \left|A'_t\right| > \left|A'_p\right| \\ 0, & otherwise \end{cases} \tag{9}$$

Step4: The entire watermark embedded in the HDR host image can be obtained by rearranging the extracted binary information.

III. EXPERIMENTAL RESULTS AND DISCUSSIONS

In order to validate the effectiveness of the proposed watermarking algorithm, 30 HDR images and 27 TM attacks are used in the test experiments. The HDR host images are selected from three sources: Greg Ward's website repository [27], Image Gallery's website repository [28] and the TMQI database [29]. The 27 TMs are selected from the HDR Toolbox of Matlab [26]. The host images and TMs are listed in Table 1 and Table 2, and Figure 7 shows all of the test images in which all images are tone-mapped using the TM_{25} for visualization purposes.

Three factors including imperceptibility, embedding capacity and robustness are usually considered when evaluating the performance of watermarking algorithm. Peak signal-to-noise ratio (PSNR) is commonly used in LDR image watermarking algorithm as an evaluation indicators of imperceptibility. However, the maximum value of pixels of an HDR image is too large, which may lead to inaccurate PSNR calculation of the HDR image. Therefore, we analytically discuss the imperceptibility of the proposed algorithm by means of the signal to noise ratio (SNR), Structural Similarity (SSIM), and HDR-VDP-2.2 [30]. The VDP is an objective quality evaluation index specifically for HDR image, which is defined as

$$VDP = \frac{1}{F.O} \sum_{f=1}^{F} \sum_{o=1}^{O} w_f \log \left(\frac{1}{I} \sum_{i=1}^{I} D_p^2 [f, o] (i) + \varepsilon \right) \tag{10}$$

where i is the pixel index, D_p denotes the noise-normalized difference between the f-th spatial frequency ($f = 1$ to F) band and o-th orientation ($o = 1$ to O) of the steerable pyramid for the host and watermarked images, $e = 10^{-5}$ is a constant to avoid singularities when D_p is close to 0, I is the total number of pixels, and w_f is the vector of per-band pooling weights. Additionally, to assess the robustness, the BER

TABLE 2. The 27 Different TM Attacks Used in Experiments [26].

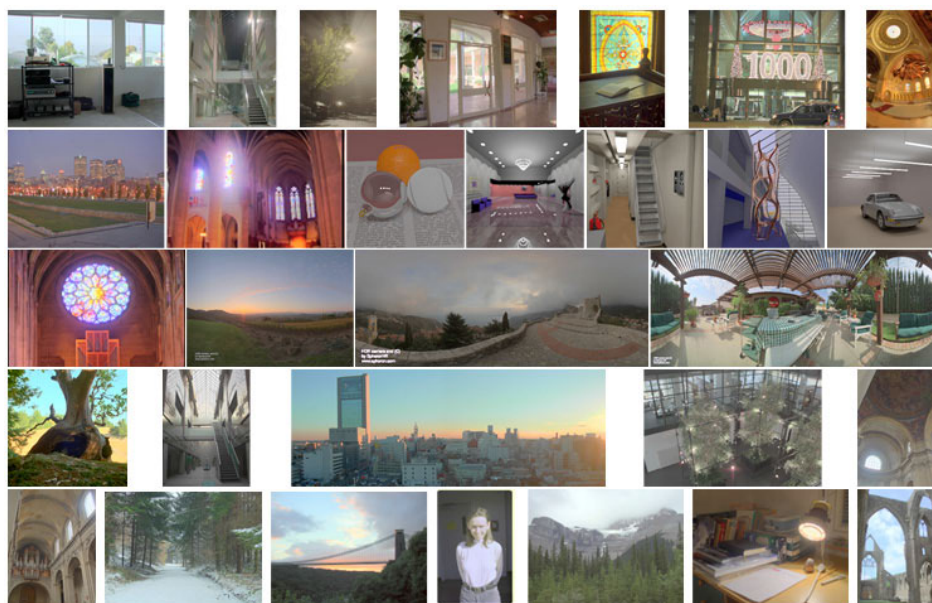| TM ID	TM Name	TM ID	TM Name	TM ID	TM Name
TM_1	Ashikhmin	TM_{10}	Gamma	TM_{19}	Raman
TM_2	Banterle	TM_{11}	KimKautzConsistent	TM_{20}	ReinhardDevlin
TM_3	BruceExpoBlend	TM_{12}	Krawczyk	TM_{21}	Reinhard
TM_4	Chiu	TM_{13}	Kuang	TM_{22}	Schlick
TM_5	Drago	TM_{14}	Lischinski	TM_{23}	TumblinRushmeier
TM_6	Durand	TM_{15}	Logarithmic	TM_{24}	VanHateren
TM_7	Exponential	TM_{16}	Mertens	TM_{25}	WardGlobal
TM_8	Fattal	TM_{17}	Normalize	TM_{26}	WardHistAdj
TM_9	Ferwerda	TM_{18}	PattanaikVisual	TM_{27}	Yee

FIGURE 7. The 30 test HDR host images rendered via the TM_{25}.

metric is selected, which is defined as

$$BER = \frac{N_e}{N_t} \times 100\% \qquad (11)$$

where N_e and N_t are the number of wrong extracted bits and the number of total watermark bits, respectively.

A. EMBEDDING CAPACITY AND IMPERCEPTIBILITY

Embedding capacity of the proposed algorithm mainly depends on the size of image block and the distribution ratio of "0" and "1" in the luminance mask. The block size N is set to 5 to ensure a certain embedding capacity in this paper. Table 3 shows the embedding payload and embedding ratio of the proposed algorithm with respect to each of the 30 test HDR host images. The average embedding payload and ratio of the 30 images are 47644bit and 0.0290bpp respectively, significantly higher than that of the most existing HDR image watermarking algorithms. Table 4 shows embedding payload, embedding ratio, SNR, SSIM, VDP, BER0 (no TM attack), BER1 (the average value of 27 TM attacks) of the 29th HDR
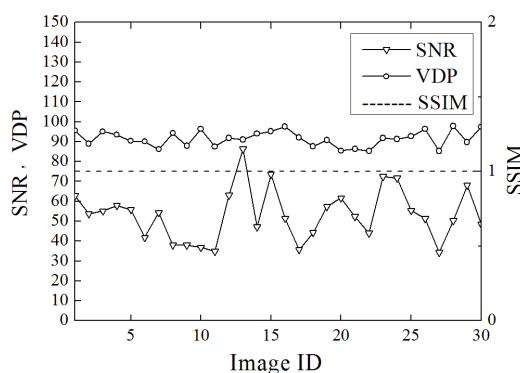

FIGURE 8. Image quality of watermarked HDR images.

host image when the block size is 3, 5 and 7, respectively. It is seen that the proposed algorithm is equally effective for other block sizes such as 3, 7, etc. In addition, the embedding capacity tends to decrease with the increase of block size, while the imperceptibility increases gradually.

TABLE 3. The embedding capacity of 30 HDR test images.

Image ID	Payload (bit)	Ratio (bpp)	Image ID	Payload (bit)	Ratio (bpp)	Image ID	Payload (bit)	Ratio (bpp)
1	85262	0.0271	11	12957	0.0392	21	114693	0.0221
2	19473	0.0252	12	39334	0.0375	22	11361	0.0164
3	19508	0.0230	13	31235	0.0298	23	121927	0.0388
4	23556	0.0299	14	38244	0.0365	24	121097	0.0385
5	15730	0.0279	15	11803	0.0342	25	66940	0.0213
6	95130	0.0302	16	171104	0.0266	26	9148	0.0240
7	15347	0.0390	17	137706	0.0397	27	6139	0.0321
8	66201	0.0210	18	98750	0.0236	28	10462	0.0274
9	13719	0.0397	19	19217	0.0229	29	12547	0.0329
10	16604	0.0158	20	19546	0.0253	30	4578	0.0213
Mean							**47644**	**0.0290**

TABLE 4. Comparison results of the 29th HDR host image with respect to different block sizes.

Block size (N×N)	Payload (bit)	Ratio (bpp)	Imperceptibility Index			Bit Error Rate	
			VDP	SNR	SSIM	BER0	BER1
3×3	36505	0.0957	82.5535	58.8404	1.0000	0.33	6.64
5×5	12547	0.0329	89.7150	67.9345	1.0000	0.02	5.29
7×7	6296	0.0165	90.0155	67.7563	1.0000	0.64	6.17

(a) HDR host image

(b) Partially enlarged HDR host image

(c) Partially enlarged watermarked HDR image

FIGURE 9. Partially enlarged view of HDR host images and their watermarked images. (a) HDR host image. (b) Partially enlarged HDR host image. (c) Partially enlarged watermarked HDR image.

In order to show the imperceptibility of the proposed algorithm, Figure 8 gives the objective image quality of the 30 watermarked HDR images. The average values of SNR, SSIM, and VDP of the 30 HDR test images are up to 53.2654dB, 1.0000 and 91.5311, respectively. It is seen that SNRs of four watermarked HDR images with Image ID of

TABLE 5. Comparison with Guerrini's [15] and Bai's [22] algorithms in capacity (bit) and BER (%).

Image ID	Algorithms	Payload (bit)	BER of watermarked HDR images processed by different TMs (%)					
			No TM	TM_5	TM_6	TM_8	TM_{18}	TM_{20}
1	Guerrini[15]	3106	16.68	23.63	36.41	41.15	25.85	30.62
	Bai[22]	51474	6.20	7.54	8.79	**14.14**	8.17	11.42
	Proposed	**85262**	**0.45**	**2.62**	6.40	20.77	**4.35**	**5.06**
2	Guerrini[15]	666	15.32	19.52	30.63	38.44	27.33	21.32
	Bai[22]	18294	3.37	4.49	4.58	**10.45**	**3.44**	7.46
	Proposed	**19473**	**0.14**	**2.64**	**1.86**	19.26	3.63	**6.47**
3	Guerrini[15]	737	13.70	17.23	27.54	37.86	23.47	16.01
	Bai[22]	**23763**	2.31	**3.35**	**2.10**	**10.65**	7.12	12.89
	Proposed	19508	**0.33**	3.78	2.69	14.99	**4.12**	**8.17**
4	Guerrini[15]	666	26.28	30.18	33.63	39.49	31.83	33.48
	Bai[22]	**28087**	6.66	8.57	8.73	**13.93**	9.02	16.56
	Proposed	23556	**0.16**	**3.20**	5.40	23.47	**3.84**	**7.07**
5	Guerrini[15]	457	26.04	32.60	35.67	38.51	36.76	41.36
	Bai[22]	**17037**	10.07	10.47	12.07	**19.48**	12.72	16.25
	Proposed	15730	**0.57**	**5.58**	**11.16**	44.21	**5.41**	**10.88**
7	Guerrini[15]	298	21.48	27.18	32.89	32.55	34.56	32.89
	Bai[22]	14788	11.62	12.07	12.39	**22.79**	15.00	16.40
	Proposed	**15347**	**0.65**	**6.23**	**11.00**	40.95	**4.18**	**14.30**
8	Guerrini[15]	3106	28.40	30.14	29.97	35.61	32.49	32.20
	Bai[22]	59505	7.87	12.17	9.02	21.29	12.18	25.97
	Proposed	**66201**	**0.31**	**2.47**	**2.37**	**18.23**	**3.93**	**5.44**
10	Guerrini[15]	938	24.63	26.12	35.39	36.35	28.68	27.40
	Bai[22]	**18761**	0.25	**0.23**	**0.72**	**0.92**	**0.52**	**0.26**
	Proposed	16604	**0.04**	1.84	2.90	17.14	1.76	2.67
19	Guerrini[15]	729	17.70	30.18	36.90	39.64	36.76	38.41
	Bai[22]	18295	12.24	15.96	14.17	**22.01**	15.44	22.30
	Proposed	**19217**	**3.41**	**5.46**	**13.25**	22.04	**12.08**	**10.45**

"10", "11", "17" and "27" are only about 35dB, which is the lowest in Figure 8. However, Figure 9 gives the partially enlarged view of these four HDR host images and their watermarked images. It is seen that human eyes still cannot perceive the obvious distortion from these four images. The above experimental results show that the imperceptibility of the proposed algorithm is satisfied.

B. ROBUSTNESS EVALUATION

In the proposed algorithm, the local correlation model and luminance mask are used to embed watermark in the first feature map of the core tensor of the host image, which not only can guarantee the imperceptibility of watermarked images, but also can avoid the problem of poor robustness in high-luminance areas. Moreover, embedding watermark in the first feature map can effectively disperse the watermark information into the three RGB channels of the host image, thus the robustness of watermark against TM attacks is improved. Figure 10 shows the average BER of each of the 30 images processed with the 27 TM attacks listed in Table 2, respectively. The average BER over 30 watermarked HDR images under each of the 27 TM attacks is also given in Figure 11. As can be seen from Figure 10, different images

have different robustness against TM attacks, mainly because these 30 test images have different specificities, such as content, size, dynamic range, etc. The average BER of the 30 watermarked HDR images is only 0.44% without TM attacks, and the average BER of the 30 watermarked HDR images attacked with different TMs is 7.13%. It is clear that the proposed algorithm is robust to TM attacks.

C. COMPARISON WITH OTHER WATERMARKING ALGORITHMS

In order to ensure rationality of the comparative experiment, the practicability, effectiveness of the algorithms, and whether the watermark extraction process is blind, etc. are considered. The proposed algorithm is compared with the Guerrini's algorithm [15], Maiorana's algorithm [20] and Bai's algorithm [22] in terms of embedding capacity and robustness against different TM attacks. The test HDR images and TM attacks selected in this experiment are consistent with those in the comparative literatures. The comparison results are given in Table 5 and Table 6, in which the bold indicates the best one.

From Table 5 and Table 6, it can be seen that the embedding capacity of the proposed algorithm is about 15 times of that

TABLE 6. Comparison with Maiorana's [20] and Bai's [22] algorithms in capacity (bit) and BER (%).

Image ID	Algorithms	Payload (bit)	BER of watermarked HDR images processed by different TMs (%)					
			No TM	TM$_5$	TM$_6$	TM$_{13}$	TM$_{20}$	TM$_{23}$
2	Maiorana[20]	1914	0.57	3.45	10.03	9.87	**4.18**	9.56
	Bai[22]	18294	3.37	4.49	4.58		7.46	
	Proposed	**19473**	**0.14**	**2.64**	**1.86**	**1.31**	6.47	**2.97**
7	Maiorana[20]	990	**0.03**	8.48	**7.17**	15.15	**5.86**	8.28
	Bai[22]	14788	11.62	12.07	12.39		16.40	
	Proposed	**15347**	0.65	**6.23**	11.00	**3.19**	14.30	**4.57**
9	Maiorana[20]	882	29.12	33.88	36.58	36.26	33.08	33.99
	Bai[22]	—	—	—	—	—	—	—
	Proposed	**13719**	**0.82**	**6.06**	**7.81**	**3.16**	**9.45**	**4.35**
11	Maiorana[20]	768	22.26	30.73	25.91	33.98	28.39	30.08
	Bai[22]	**13656**	8.16	8.60	9.32	8.57	8.37	8.25
	Proposed	12957	**1.46**	**8.20**	**7.74**	**5.13**	**8.13**	**7.35**
13	Maiorana[20]	2700	22.22	30.44	27.70	32.81	24.19	30.22
	Bai[22]	**42093**	0.82	**0.95**	**2.06**	**2.99**	**1.83**	**1.34**
	Proposed	31235	**0.06**	6.14	8.41	6.73	10.38	6.51
15	Maiorana[20]	882	19.59	28.89	32.06	36.26	30.36	32.29
	Bai[22]	**12867**	9.25	10.32	9.63	11.22	21.05	10.70
	Proposed	11803	**0.05**	**4.85**	**6.79**	**4.06**	**14.32**	**6.64**
20	Maiorana[20]	1914	**0.16**	6.95	23.77	14.84	**7.21**	23.98
	Bai[22]	19527	4.86	5.22	6.07	5.84	9.34	8.51
	Proposed	**19546**	0.36	**3.20**	**5.54**	**2.33**	10.72	**1.77**
21	Maiorana[20]	13407	**0.16**	35.46	21.17	5.91	**4.97**	6.86
	Bai[22]	60983	5.58	9.76	9.72	17.71	18.69	4.96
	Proposed	**114693**	0.34	**3.34**	**5.85**	**3.38**	23.56	**1.78**
22	Maiorana[20]	1710	1.23	4.27	19.71	12.98	**4.56**	14.68
	Bai[22]	10788	4.34	4.29	5.10	4.75	7.57	7.82
	Proposed	**11361**	**0.93**	**3.35**	**3.41**	**4.45**	12.14	**1.47**
23	Maiorana[20]	8100	6.69	25.26	15.33	31.26	18.68	19.38
	Bai[22]	**129508**	4.23	6.47	4.61	5.64	24.35	17.53
	Proposed	121927	**0.16**	**5.17**	**3.31**	**2.90**	**14.24**	**2.59**
24	Maiorana[20]	8100	12.11	26.11	23.86	23.42	20.42	23.02
	Bai[22]	**124668**	4.71	5.89	5.20	5.18	15.83	8.00
	Proposed	121097	**0.18**	**5.87**	**5.10**	**3.78**	**13.91**	**2.25**
25	Maiorana[20]	8100	0.17	10.38	19.23	5.42	**6.96**	14.79
	Bai[22]	48081	8.83	10.73	9.07	13.90	13.46	15.65
	Proposed	**66940**	**0.01**	**3.82**	**5.63**	**3.95**	14.33	**1.69**

TABLE 7. Comparison of comprehensive performance.

Algorithms		Guerrini [15]	Maiorana [20]	Bai [22]	Proposed
Number of test images		15	15	30	30
Number of TMs		7	6	27	27
Average of BER(%)	No TM	21.81	9.60	5.57	0.44
	TMs	30.02	21.81	8.72	7.13
Payload (bit)		298-3106	768-13407	10^4-10^5	10^3-10^5

of Guerrini's and Maiorana's algorithms, and is equivalent to that of Bai's algorithm. In terms of robustness, although BERs of a few images of the proposed algorithm are higher than that of comparative algorithms, most of BERs are lower than that of the Guerrini's and Maiorana's algorithms.

Moreover, Table 7 shows the comparison results of comprehensive performance between the proposed algorithm and the comparative algorithms. It can be seen that compared with literature [15] and literature [20], more test images and TM attacks are tested in the experiments, and the proposed
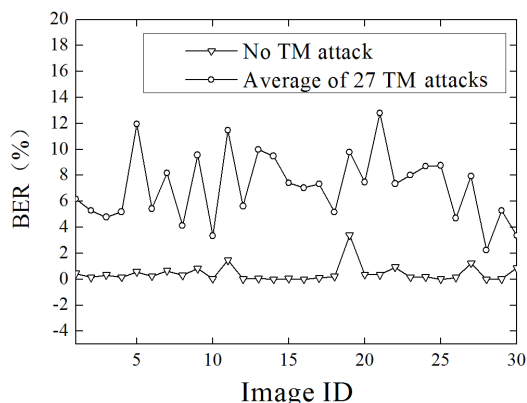
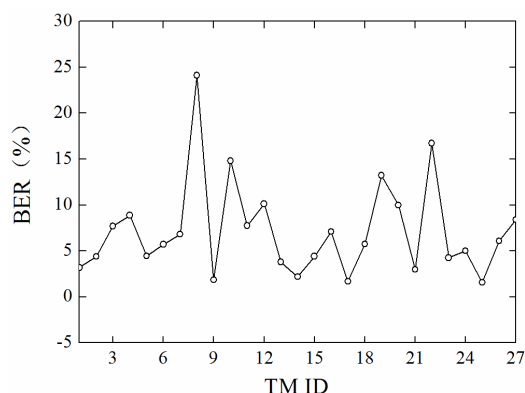**FIGURE 10.** Average BER of each of 30 watermarked images over 27 TM attacks.

FIGURE 11. Average BER of each of 27 TM attacks over 30 watermarked HDR images.

algorithm achieves higher embedding capacity and better robustness.

IV. CONCLUSION

In this paper, a highly robust HDR image watermarking algorithm against TM attacks is proposed, which benefits from Tucker decomposition, local correlation model, luminance mask and embedding intensity selection strategy. Firstly, considering that the first feature map of the core tensor has good stability, and the watermark embedded in the first feature map can easily be spread to the three RGB channels of the HDR host image through inverse Tucker decomposition, the proposed algorithm embeds watermark based on Tucker decomposition, so as to avoid the damage of the internal structure of the data caused by embedding watermark into single channel of the host image, as well as to improve the robustness of watermark against different TM attacks. Furthermore, a low-complexity luminance masking approach and a local correlation model based on AR prediction are designed for further improving the robustness of the watermark and reducing the probability of poor imperceptibility caused by inaccurate prediction. Finally, an embedding intensity selection strategy is proposed to balance the imperceptibility and robustness.

The experimental results show that the proposed algorithm not only has good robustness against various different TM attacks, but also achieves good results in imperceptibility and embedding capacity. It is known that the effective use of human visual perception characteristics of an image is helpful to enhance the imperceptibility and robustness of the watermarking algorithm. But this work barely takes that into consideration because the human visual perception characteristics of HDR image is undoubtedly different from that of the LDR image. Thus in the future, how to mine the human visual perception characteristics of HDR image and apply it to digital watermarking technology of HDR image is a problem worth studying.

REFERENCES

[1] V. Hulusic, K. Debattista, G. Valenzise, and F. Dufaux, "A model of perceived dynamic range for HDR images," *Signal Process., Image Commun.*, vol. 51, pp. 26–39, Feb. 2017.

[2] F. Guan, G. Jiang, Y. Song, M. Yu, Z. Peng, and F. Chen, "No-reference high-dynamic-range image quality assessment based on tensor decomposition and manifold learning," *Appl. Opt.*, vol. 57, no. 4, pp. 839–848, Feb. 2018.

[3] Y. Song, G. Jiang, H. Jiang, M. Yu, F. Shao, and Z. Peng, "A new tone-mapped image quality assessment approach for high dynamic range imaging system," in *Proc. IEEE Int. Conf. Image Process.*, Beijing, China, Sep. 2017, pp. 1012–1016.

[4] A. Nayana and A. K. Johnson, "High dynamic range imaging—A review," *Int. J. Image Process.*, vol. 9, no. 4, pp. 198–208, 2015.

[5] A. Artusi, T. Richter, T. Ebrahimi, and R. K. Mantiuk, "High dynamic range imaging technology," *IEEE Signal Process. Mag.*, vol. 34, no. 5, pp. 165–172, Sep. 2017.

[6] D. Kundu, D. Ghadiyaram, A. C. Bovik, and B. L. Evans, "Large-scale crowdsourced study for tone-mapped HDR pictures," *IEEE Trans. Image Process.*, vol. 26, no. 10, pp. 4725–4740, Oct. 2017.

[7] N. Agarwal, A. K. Singh, and P. K. Singh, "Survey of robust and imperceptible watermarking," *Multimedia Tools Appl.*, vol. 78, no. 7, pp. 8603–8633, Apr. 2019.

[8] C.-M. Yu, K.-C. Wu, and C.-M. Wang, "A distortion-free data hiding scheme for high dynamic range images," *Display*, vol. 32, no. 5, pp. 225–236, Dec. 2011.

[9] Z.-H. Wang, T.-Y. Lin, C.-C. Chang, and C.-C. Lin, "A novel distortion-free data hiding scheme for high dynamic range images," in *Proc. 4th Int. Conf. Digit. Home*, Guangzhou, China, Nov. 2012, pp. 33–38.

[10] C.-C. Chang, T.-S. Nguyen, and C.-C. Lin, "Distortion-free data embedding scheme for high dynamic range images," *J. Electron. Sci. Technol.*, vol. 11, no. 1, pp. 20–26, 2013.

[11] C.-C. Chang, T.-S. Nguyen, and C.-C. Lin, "A new distortion-free data embedding scheme for high-dynamic-range images," *Multimedia Tools Appl.*, vol. 75, no. 1, pp. 145–163, Jan. 2016.

[12] Y.-M. Cheng and C.-M. Wang, "A novel approach to steganography in high–dynamic-range images," *IEEE Multimedia*, vol. 16, no. 3, pp. 70–80, Jul./Sep. 2009.

[13] M.-T. Li, N.-C. Huang, and C.-M. Wang, "A data hiding scheme for high dynamic range images," *Int. J. Innov. Comput. Inf. Control*, vol. 7, no. 5A, pp. 2021–2035, May 2011.

[14] Y.-T. Lin, C.-M. Wang, W.-S. Chen, F.-P. Lin, and W. Lin, "A novel data hiding algorithm for high dynamic range images," *IEEE Trans. Multimedia*, vol. 19, no. 1, pp. 196–211, Jan. 2017.

[15] F. Guerrini, M. Okuda, N. Adami, and R. Leonardi, "High dynamic range image watermarking robust against tone-mapping operators," *IEEE Trans. Inf. Forensics Security*, vol. 6, no. 2, pp. 283–295, Jun. 2011.

[16] X. Xue, T. Jinno, X. Jin, M. Okuda, and S. Goto, "Watermarking for HDR image robust to tone mapping," *IEICE Trans. Fundam. Electron. Commun. Comput. Sci.*, vol. E94-A, no. 11, pp. 2334–2341, Nov. 2011.

[17] J. Wu, "Robust watermarking framework for high dynamic range images against tone mapping attacks," in *Watermarking*, vol. 2, M. D. Gupta, Ed. Rijeka, Croatia: InTech, 2012, [Online]. Available: http://www.intechopen.com/books/watermarking-volume-2/robust-watermarking-framework-for-high-dynamic-range-images-against-tone-mapping-attacks

[18] V. Solachidis, E. Maiorana, P. Campisi, and F. Banterle, "HDR image watermarking based on bracketing decomposition," in *Proc. 18th Int. Conf. Digit. Signal Process.*, Santorini, Greece, Jul. 2013, pp. 1–6.

[19] V. Solachidis, E. Maiorana, and P. Campisi, "HDR image multi-bit watermarking using bilateral-filtering-based masking," *Proc. SPIE*, vol. 8655, Feb. 2013, Art. no. 865505.

[20] E. Maiorana and P. Campisi, "High-capacity watermarking of high dynamic range images," *EURASIP J. Image Video Process.*, vol. 2016, no. 1, p. 3, Dec. 2016.

[21] G. Anbarjafari and C. Ozcinar, "Imperceptible non-blind watermarking and robustness against tone mapping operation attacks for high dynamic range images," *Multimedia Tools Appl.*, vol. 77, no. 18, pp. 24521–24535, Sep. 2018.

[22] Y. Bai, G. Jiang, M. Yu, Z. Peng, and F. Chen, "Towards a tone mapping-robust watermarking algorithm for high dynamic range image based on spatial activity," *Signal Process., Image Commun.*, vol. 65, pp. 187–200, Jul. 2018.

[23] B. W. Bader and T. G. Kolda, "Algorithm 862: MATLAB tensor classes for fast algorithm prototyping," *ACM Trans. Math. Softw.*, vol. 32, no. 4, pp. 635–653, Dec. 2006.

[24] Z. Xiaoli, L. Xiongfei, F. Yuncong, Z. Haoyu, and L. Zhaojun, "Image fusion with internal generative mechanism," *Expert Syst. Appl.*, vol. 42, no. 5, pp. 2382–2391, Apr. 2015.

[25] Y. Huo and F. Yang, "High-dynamic range image generation from single low-dynamic range image," *IET Image Process.*, vol. 10, no. 3, pp. 198–205, Mar. 2016.

[26] F. Banterle. (2016). *HDR Toolbox for MATLAB, Version: 1.1.0.* [Online]. Available: https://github.com/banterle/HDR_Toolbox

[27] *Anyhere Software Database*. Accessed: 2003. [Online]. Available: http://www.anyhere.com/gward/hdrenc/pages/originals.html

[28] *Image Gallery*. Accessed: 2018. [Online]. Available: http://resources.mpi-inf.mpg.de/hdr/gallery.html

[29] *Subject-Rated Image Database of Tone-Mapped Images*. Accessed: 2013. [Online]. Available: https://ece.uwaterloo.ca/~z70wang/research/tmqi

[30] M. Narwaria, R. Mantiuk, M. P. Da Silva, and P. Le Callet, "HDR-VDP-2.2: A calibrated method for objective quality prediction of high-dynamic range and standard images," *Proc. SPIE*, vol. 24, no. 1, Jan. 2014, Art. no. 010501.

YANG WANG received the B.S. degree from Ningbo University, Ningbo, China, in 2016, where she is currently pursuing the M.S. degree. Her current research interests include digital watermarking and image processing.

GANGYI JIANG received the M.S. degree from Hangzhou University, China, in 1992, and the Ph.D. degree from Ajou University, South Korea, in 2000. He is currently a Professor with the Faculty of Information Science and Engineering, Ningbo University, China. He has authored over 100 technical articles in refereed journals. His research interests include visual communication and image/video processing, 3D video coding, omni-directional video processing, light field imaging, visual perception, and quality assessment.

YONGQIANG BAI received the B.S. and M.S. degrees from Zhengzhou University, in 2006 and 2009, respectively. He is currently pursuing the Ph.D. degree with the Ningbo University. His research interests include data hiding, digital watermarking, and image processing.

MEI YU received the B.S. and M.S. degrees from the Hangzhou Institute of Electronics Engineering, China, in 1990 and 1993, respectively, and the Ph.D. degree from Ajou University, South Korea, in 2000. She is currently a Professor with the Faculty of Information Science and Engineering, Ningbo University, China. Her research interests include image/video coding and visual perception.

TING LUO received the B.Sc. degree in computer science from Ningbo University, Ningbo, China, in 2003, the M.Sc. degree in business information technology from Middlesex University, London, U.K., in 2004, and the Ph.D. degree from Ningbo University, in 2015. His research interests include multimedia security, image processing, data hiding, and pattern recognition.

• • •